LAWRENCE
LIVERMORE
NATIONAL
LABORATORY

UCRL-JRNL-211413

The Melting Curve and High-Pressure Chemistry of Formic Acid to 8 GPa and 600 K

W. Montgomery, J. M. Zaug, W. M. Howard, A. F. Goncharov, J. C. Crowhurst, R. Jeanloz

April 15, 2005

Journal of Physical Chemistry B

Disclaimer

The Melting Curve and High-Pressure Chemistry of Formic Acid to 8 GPa and 600 K

W. Montgomery[1], J. M. Zaug[2], W. M. Howard[2], A. F. Goncharov[2], J. C. Crowhurst[2], and R. Jeanloz[1]*

[1*]Department of Earth and Planetary Science, University of California, Berkeley, 307 McCone Hall, Berkeley, CA 94720-4767

wren@eps.berkeley.edu

Melting Curve and chemistry of HCOOH

[2]University of California at Lawrence Livermore National Laboratory, Chemistry & Material Science Directorate, 7000 East Avenue, Livermore, CA 94551

ABSTRACT: We have determined the melting temperature of formic acid(HCOOH) to 8.5 GPa using infrared absorption spectroscopy, Raman spectroscopy and visual observation of samples in a resistively heated diamond-anvil cell. The experimentally determined melting curve compares favorably with a two-phase thermodynamic model. Decomposition reactions were observed above the melting temperature up to a pressure of 6.5 GPa, where principal products were CO_2, H_2O and CO. At pressures above 6.5 GPa, decomposition led to solid-like reaction products. Infrared and Raman spectra of these recovered products indicate that pressure affects the nature of carbon-carbon bonding.

Introduction

As the simplest carboxyl molecule, formic acid (O=CH–OH) offers an archetype for characterizing the effects of pressure on the hydrogen bonding, polymerization and chemical kinetics of organic compounds. It is also of interest for understanding the origination of life, because it is among the simplest "pre-biotic" molecules present in space, and has been observed in spectra from the interstellar medium, from around

protostars and comets and in meteorites (*i. e.*, remnants of the building blocks of planets) [1-7]. Pressure is relevant here because life can potentially be established more readily at depth, within a planetary body, than on the planetary surface where the pre-biotic molecules are subject to the destructive effects of high velocity impact from extra-planetary bolides and of ionizing radiation from space (unless a sufficiently dense atmosphere is present). Formic acid is also considered an important reaction intermediate in "maturation" – that is, heating under pressure – of organic matter beneath the Earth's surface [8].

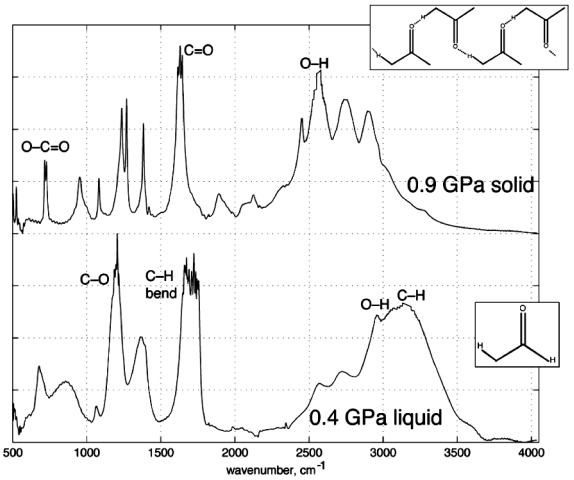

Figure 1: Comparison of infrared absorption spectra of single-crystal (top) and of liquid (bottom) formic acid obtained at 298 K and at 0.9 GPa and 0.4 GPa, respectively. Band assignments follow [9], and insets illustrate molecular structures.

Unlike other carboxylic acids, HCOOH does not form dimers in the liquid and solid states[9]. It instead forms an infinite network of hydrogen-bonded chains, which are linked by a hydroxyl group displaying a characteristic infrared-absorption band at ~2600 cm^{-1} (Figure 1). Crystallization at ambient temperature and low pressure (< 1GPa) evidently involves forming links between the chains, as indicated by the observed softening of the O–H vibration frequency (the absorption peak shifts from ~3000 cm^{-1} to ~2600 cm^{-1}).

A phase transition was previously reported to occur at 4.5 GPa and 300 K [9], and a subsequent single-crystal diffraction study proposed a high-pressure crystal structure consisting of a more complex phase combining *cis*- and *trans*- isomers of HCOOH in symmetrically flat layers [10]. Recent powder x-ray diffraction data indicate that the low-pressure phase is stable to well over 30 GPa at 300 K, however, and we consequently do not consider solid-solid phase transformations in the present study [11].

Experimental Methods

Pure formic acid was obtained starting from 98% HCOOH, to which pthalic anhydride was added and the mixture refluxed (6 hr under a dry atmosphere) and twice distilled (97-99 ˚C and 99-100˚ C). Aliquots were then loaded into a membrane-type diamond-anvil cell containing type II diamonds with 500 μm culets [12]. A pure Ir gasket with an initial thickness of ~30 microns and 220 μm diameter sample chamber was used to contain each sample. Samples were heated at rates of less than 0.05 K/min to more than 1 K/min, using a Eurotherm 2408 electronic temperature-control system powering an external heating ring that surrounds the diamond cell.

We made spectroscopic measurements during both heating and cooling cycles. This, combined with visual observation of liquification and crystallization, allowed us to determine the melting curve of formic acid as a function of pressure (Fig 1). Fourier-transform infrared (FTIR) absorption and Raman spectra were obtained through a long working-distance microscope designed to accommodate heated diamond cells. Our FTIR system consists of a Bruker Optics Vector-33 interferometer and a glowbar source, in conjunction with liquid-nitrogen cooled InSb and HgCdTe detectors, for complete coverage of the spectral ranges of interest. Raman and fluorescence spectra are fiber injected into a 0.8 m focal length spectrometer and dispersed using an 1800 lines/mm grating onto a thermoelectrically cooled CCD multichannel array. The IR resolution was selected to be 4 cm^{-1}. We monitored pressure during heating and cooling using the $SrB_4O_7:Sm^{2+}$ $\lambda_{0\text{-}0}$ [13] and/or the temperature-dependant ruby ($Al_2O_3:Cr^{3+}$) fluorescence lines [14]. Temperature is monitored using type-K thermocouples from Omega Engineering secured against the gasket and one of the diamond anvils with gold foil. The temperature precision is ±0.5 K, but the absolute accuracy decreases with increasing temperature, due to the high thermal conductivity of diamond, and was estimated to be +0 K and –4 K up to 575 K. The sample pressure was maintained to within 0.2 GPa throughout each experiment by monitoring the pressure gauge and adjusting the DAC membrane pressure accordingly.

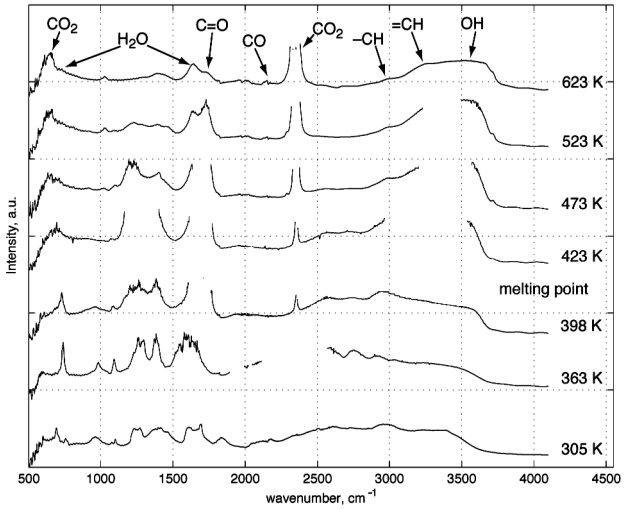

Figure 2: Selection from a series of time-resolved FTIR spectra of pure formic acid at 3.0 GPa and a heating rate of 1 K/min (bottom to top). Complete solid-liquid transition is observed at ~423 K, with the formation of a broad O-H peak at ~3450 cm^{-1} and the disappearance of the O-C-O torsional band at 680 cm^{-1}. CO_2 formation (strong band at 2350 cm^{-1}) is observed at 398 K, concurrent with the visual appearance of liquid. Above 500 K, a δ-CO doublet is visible at 2130 cm^{-1} and 2148 cm^{-1}. The formation of H_2O is determined by the appearance of secondary H_2O bands at 1620 cm^{-1} and a shoulder at ~600 cm^{-1}. Gaps in the spectra indicate regions of total absorption by the sample.

Results

A. Solid-liquid transformation

Figure 2 shows spectra acquired at a fixed pressure of 3.0 GPa, and a constant heating rate of 1 K/min from 300 K to 623 K. At 423 K, the hydroxyl peak at 3000 cm^{-1} shifts in position and intensity to a broad band at ~3500 cm^{-1}, indicating the formation of liquid HCOOH which was confirmed by visual inspection (cf. Fig. 1).

Melting temperatures were determined in this manner, through a combination of spectroscopic measurements and visual observation, over a range of pressure up to 8 GPa. In order to determine the equilibrium fusion curve, and overcome possible kinetic barriers, samples were characterized both on heating (melting) and cooling (crystallization) at different rates. Figure 3 illustrates such an experiment, with the sample heated and then cooled (not shown) at the slower rate of 0.05 K/min while at 3.4 GPa. A similar spectral evolution is documented, and the fact that melting occurs at a lower temperature than for the 1 K/min heating rate (as also confirmed by visual observation) demonstrates that data collected at the faster

heating rate provides only an upper bound on the melting curve due to kinetic hindrances (i.e., superheating).

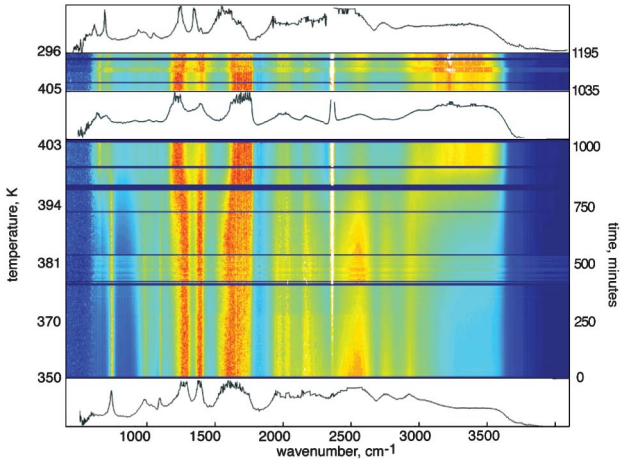

Figure 3: Time-resolved FTIR absorption spectra of pure formic acid at 3.4 GPa, heated at a rate of 0.05 K/min (bottom to top). Spectra are shown at 350 and 403 K, and then at 296 K on cooling, with color contours indicating the time evolution in between (red for high absorption, blue for low absorption). In this case, formation of (solid) CO_2 is apparent at 360 K (white saturated band), while the sample appears solid both visually and spectroscopically up to 400 K. Only a small amount of carbon dioxide is formed (~ 5% estimated from band intensities at 400K), and we find no Raman-spectroscopic evidence for the presence of molecular hydrogen, probably due to the increasing thermal background and the limitations of our spectrometer.

The present experimental constraints on the melting curve of formic acid are summarized in Fig. 4. Both undercooling and superheating are reduced significantly by decreasing the rate at which temperature is changed, with the data suggesting that the fusion temperature is bracketed to better than ±20-30 K up to 8 GPa.

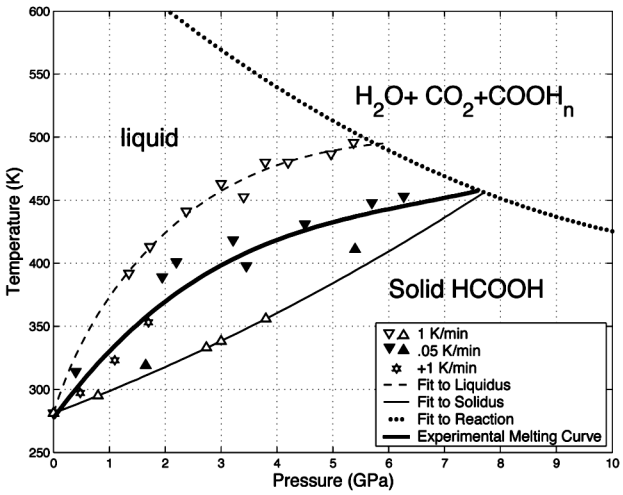

Figure 4: Solid triangles indicate upper bounds (downward pointing) and lower bounds (upward pointing) of the liquid–solid phase transition determined by slow heating/cooling rates of 0.05 K/min. Open triangles represent boundaries determined by rapid heating/cooling (1 K/min.). The experimental melting curve (solid line) represents the average of experimental results upon slow heating and cooling.

B. *High-temperature decomposition of formic acid*

The formation of simple hydrocarbons (C_2H_2, C_2H_4 and CH_4) from thermal decomposition of formic acid has been established by Muller and Petryal [15] at room pressure and high temperature (1696 K). At high pressures, we have also observed reactions on heating liquid or solid HCOOH, and the products can be quenched to ambient conditions: Fig. 5. The spectra indicate that the molecular structure and bonding of the high-temperature reaction products varies with synthesis pressure, incorporating C=O and C=C bonds at lower pressures while the higher-pressure product shows no evidence of O–O bonds and C–C bonds. These spectra, combined with visual observations, suggest that compression and heating of HCOOH results in the production of macromolecules containing C, H and O as well as the easily-detected CO_2. It is interesting to note that the spectral features from the recovered solid-like products rule out the presence of formaldehyde, HCO free radicals, formate species (HCOO), furan, butadiene, or acetylene.

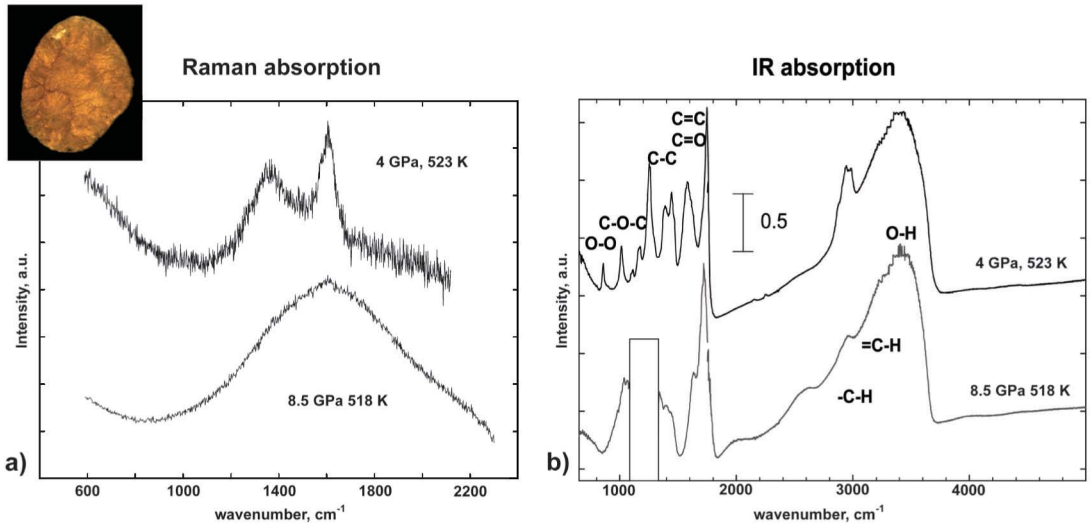

Figure 5: Raman (a) and infrared absorption (b) spectra of the C-H bend region of two different products recovered from formic acid after heating at high pressures: up to 523 K at 4 GPa (i. e., from the liquid state) and up to 518 K at 8.5 GPa (from the solid state). The spectra were all collected at ambient conditions (P = 0 GPa and T = 298 K), and show evidence of sp^2 bonding in the 4 GPa sample and sp^3 bonding (and C–C and C=C bonds at indicated by peaks at 1027 cm^{-1} and 1585 cm^{-1} respectively) in the sample quenched from 8.5 GPa. The inset is a photomicrograph of the 4.0 GPa product, which is intensely orange. These results are from separate experiments than those summarized in Fig. 4.

C. *Chemical reactions associated with the decomposition of formic acid*

Figure 6 includes two curves indicating the chemical decomposition of formic acid. Two reactions have been observed in this work, decarboxylation at approximately the temperature of melting and, below 5 GPa, dehydration at temperatures above the melting point. Figure 2 shows IR absorption spectra documenting both of these reactions: the appearance of a strong band at 2350 cm-1 at 398 K indicates the presence of CO_2, while the appearance of the bending and translational peaks of water (1620 cm-1 and 600 cm-1, respectively) along with a shift in the shape of the O-H band at ~3450 cm-1 indicates the formation of water at 623 K.

Although we did not prove that equilibrium was fully achieved in our experiments, comparisons with independent work does suggest a coherent picture. Specifically, both reactions have been observed in previous studies at 1 atm and elevated temperatures, and the decarboxylation reaction has been observed at

pressures up to 275 bar under hydrothermal conditions [16]. Our experiments on solid and liquid formic acid at high temperatures are consistent with these hydrothermal studies.

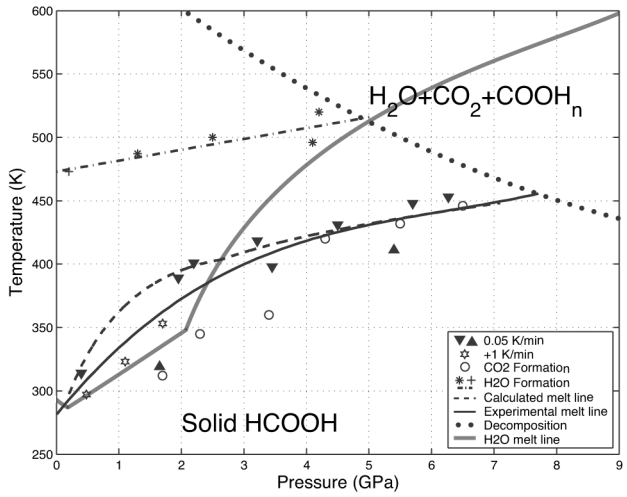

Figure 6: Experimentally determined phase and reaction diagram of formic acid, with solid and dashed lines indicating the experimental and theoretical melting curve (solid grey curve is the melting line for H_2O) and the dotted lines indicating reaction boundaries. Solid triangles indicate upper and lower bounds of the liquid-solid phase transition determined by slow heating/cooling rates of 0.05 K/min. A high-temperature chemical transformation to solid opaque products (…) is distinguished from the decomposition of formic acid into CO_2 (and inferred H_2) which occurs near the melting line (•), and the higher-temperature decomposition of formic acid into H_2O and CO at pressures below 5 GPa (*). (+) data point taken from [17].

Discussion

Figure 6 summarizes the phase- and reaction-diagram of HCOOH, as determined from our high-pressure experiments.

The melting curve is terminated at nearly 8 GPa by the high-temperature reactions we have documented for formic acid (Fig. 5). A reaction boundary is indicated by a single line, assuming that the reactions are continuously evolving with pressure so as to be in accord with our observation that different products are quenched from different pressures.

The high-temperature reactions under pressure are thus distinct from the zero-pressure decomposition, no doubt because of the strong effect of pressure on the simple-hydrocarbon reaction products in the latter case. Indeed, the spectra of the highest-pressure reaction products bear many similarities with the carbon sub-oxide spectra obtained from carbon monoxide quenched from pressures of 5 GPa [18]. Based on band assignments of our spectra as well as theoretical studies of the CO reaction products, we infer that formic acid does react to form polymeric sub-oxides at elevated pressures and temperatures [19].

For comparison with our experimental results, we have calculated a melting curve for formic acid based on minimizing the two-phase (liquid–solid) Gibbs free energy of formic acid. The model combines equation-of-state and thermochemical measurements, and has been adjusted to fit available high-pressure experimental data including shock-Hugoniot measurements [20], static-compression volumes from x-ray diffraction [11] and impulsive light-scattering determinations of sound velocities [21]. We separate the Gibbs free energy into a reference component at one atmosphere, $G_0(T)$, and a pressure-dependent component, ΔG(P). The reference values of enthalpy and entropy, which determine $G_0(T)$, are given by the heat capacity at one atmosphere ($C_{p,0}(T)$):

$$H_0(T) = \Delta H_0 + \int_{T_0}^{T} C_{p,0}(T)\, dT \qquad (1)$$

$$S_0(T) = \Delta S_0 + \int_{T_0}^{T} \frac{C_{p,0}(T)}{T}\, dT. \qquad (2)$$

We assume that in the liquid phase the heat capacity is independent of temperature, and in the solid phase we assume a single Einstein oscillator with Debye temperature Θ is set to 281 K,

$$C_{p,0}(T) = 7.5R * E(\Theta/T) \text{ where } E(x) \equiv \frac{x^2 e^x}{(e^x - 1)^2}$$

In the limit T → ∞, it can beshown C_p = 124.717 J/mole·K or 15R. Performing the integration in equations (1) and (2) yields

$$H_0(T) = \Delta H_0 + \theta \left[\frac{1}{e^x - 1} \right]_{x_0}^{x} \text{ where } x \equiv \Theta/T \text{ and } x_0 \equiv \Theta/T_0. \qquad (3)$$

$$S_0(T) = \Delta S_0 \left[\frac{x}{e^x - 1} - \ln(1 - e^x) \right]_{x_0}^{x} \qquad (4)$$

Given the relatively low melting temperature of formic acid to 6 GPa, we set the thermal expansion to zero thus resulting in a simplified expression for the high-pressure Gibbs free energy component. To calculate the pressure-dependent component of the Gibbs free energy, we use the Murnaghan equation of state, which is derived by assuming a linear pressure dependence for the bulk modulus:

$$V(P) = V_0\left[n\kappa_0 P + 1\right]^{-1/n} \qquad (5)$$

The pressure dependant component of the Gibbs free energy follows from $\Delta G = VdP - SdT$:

$$\Delta G(P) = \int_{P_0}^{P} V(P)\, dP. \qquad (6)$$

The thermodynamic values that best minimize G(P,T) to all available experimental data are provided in Table 1, with the heat capacity for the liquid being taken from JANAF tables while that for the solid being from ref [20]. The enthalpy and entropy for the liquid at STP are also taken from experimental data [22, 23], as is V_o [11]. The enthalpy and entropy of the solid are determined by replicating the melt temperature and enthalpy of melting at 1 atm pressure. The value of V_o for the solid is determined by an extrapolation of the static compression data [11] to 1 atmosphere. The B_o and n for the solid are fit simultaneously to the static-compression data and the initial slope of the measured melt curve. Likewise, the value of B_o and n values for the liquid-phase are fit to sound speed data [21] and the initial slope of the experimental melt curve (*i. e.*, the ratio of volume change to entropy change on fusion at one atmosphere). The relatively high error in fitting sound-speed data was due to the compromise required in order to derive the model parameters by fitting the measured slope of the melt curve.

Being limited to two phases, the model necessarily assumes congruent melting between solid and liquid, yet it is found to be in good agreement with our measurements (Fig. 6). The approximations underlying our model are mitigated by our having fit experimental data in order to derive optimal parameter values (Table 1). Despite its empirical basis, however, this model is not constrained to fit the high-pressure melting curve but instead does predict this curve based on the one atmosphere properties of liquid and crystalline formic acid. The good agreement with our measurements therefore documents how successful such a thermodynamic model can be despite its inherent simplifications.

Conclusions

Using FTIR and visual observation, we have determined the melting curve of formic acid to 8 GPa and 600 K, and have characterized the decomposition reactions and chemical transformations that occur up to this pressure range. The observed melting curve is reliably predicted by a simple two-phase model that is constrained by zero-pressure experimental data available prior to our study. Therefore, similar models may prove useful for predicting the melting curves of other organic compounds as a function of pressure.

As HCOOH is known to be a component of Jupiter's moons, the stability of formic acid at interior pressures and temperatures is of interest to understanding pre-biotic environments in planetary science. At the base of the "oceans" or liquid mantles of Europa and Ganymede, the pressure temperature conditions are predicted to be between 0.1-1.5 GPa and 300-1500 K [24, 25]. The cores of these moons could reach pressures up to 5 GPa. It is possible that at the base of the ocean or in inclusions in the upper core, formic acid could chemically react to form suboxides. In particular, the formation of a suboxide at elevated temperatures involves the development of a more complex, polymerized structure from the simple dimer. High-pressure studies of longer organic molecules, especially those containing benzene rings, show formation of helices and complex (double or conjugated bonds) polymers [26], suggesting that formic acid could ultimately lead to sugars and other pre-cursors of life [27].

Acknowledgements

The authors appreciate technical assistance provided by D. W, Hansen and Phil Pagoria and continued support of our work by R. L. Simpson and L. J. Terminello. We thank C. E. Young for providing the $SrB_4O_7:Sm^{2+}$ pressure marker used in this study. W. M. is supported by a LLNL EMC fellowship. This work was performed under the auspices of the U.S. Department of Energy by the University of California, Lawrence Livermore National Laboratory under contract No. W-7405-Eng-48.

Bibliography

(1) A. H. Delsemme, *Phil Trans. R. Soc. Lond.* **A 325**, 509-523 (1988).

(2) P. Ehrenfreund and S. B. Charnley, *Ann. Rev. Astron. Astrophys.* **38**, 427-83 (2000).

(3) D. Bockelee-Morvan, D. C. Lis, J. E. Wink, et al., *Astron. Astrophys.*, **353**, 1101-14 (2000).

(4) J. V. Keane, A. G. G. Thielens, A. C. A. Boogert, W. A. Schutte and D. C. B. Whittet, *Astron. Astrophys.* **376**, 254-270 (2001).

(5) S.-Y. Liu, J. M. Girart, A. Remijan and L. E. Snyder, *Astrophys. J.*, **576**, 255-263 (2002).

(6) J. M. Hollis, J. A. Pedelty, L. E. Snyder, P. R. Jewell, F. J. Lovas, P. Palmer and S. Y. Liu, *Astrophys. J.*, **588**, 353-359 (2003).

(7) S. Cazaux, A. G. G. M. Thielens, C. Ceccarelli, A. Castets, V. Wakelam, E. Caux, B. Parise and D. Teyssier, *Astrophys. J.*, **593**, L51-L55 (2003).

(8) T. M. McCollom and J. S. Seewald, Geochim. *Cosmochim. Acta*, **67**, 3625-3644 (2003).

(9) H. Shimizu, *Physica*, **139**, 479 (1986).

(10) D. R. Allan and S. J. Clark, *Phys. Rev. Lett.* **82**(17), 3464 (1999).

(11) A. F. Goncharov, M. R. Manaa, J. M. Zaug, R. H. Gee, L. E. Fried and W. Montgomery, *Phys. Rev. Lett.* **94**, 065505 (2005).

(12) J. C. Chervin, B. Canny, J. M. Besson, and Ph. Pruzan, *Rev. Sci. Instrum.* **66** (3) 2595-2598 (1995).

(13) F. Datchi, R. LeToullec, and P. Loubeyre, *J. Appl. Phys.* **81** (8), 3333 (1987).

(14) H. K. Mao, J. Xu, and P. M. Bell, *J. Geophys. Res.* **91**, 4673 (1986).

(15) J. A. Muller and E. Peytral, *Memoires Presentes a la Societe Chemique*, **34** (1920).

(16) P. G. Maiella, and T. B. Brill, J. Phys. Chem., **102** (29), 5886 (1998).

(17) A. Sharma, G. Cody, R. M. Hazen, and R. J. Hemley *EoS Trans supp*, **81** (19), S52 (2000).

(18) M. Lipp, W. J. Evans, V. Garcia-Baonza, and H. E. Lorenzana, *J. Low Temp. Phys.*, **111**, 247 (1998).

(19) S. Bernard, G. L. Chiarotti, S. Scandolo and E. Tosatti, *Phys. Rev. Lett.*, **81**, 2092 (1998).

(20) R. F. Trunin, M. V. Zhernokletoc, N. F. Kuznetsov, O. A. Radchenko, N. V. Sychevskaya, and V. V. Shutov, *Khim. Fiz.* **11**(3), 424 (1992)

(21) J. C. Crowhurst, J. M. Zaug, L. E. Fried et al., submitted for publication (2004).

(22) R.C. Wilhoit, J. Chao, and K. R. Hall, *J. Phys. Chem Ref. Data* **14**(1), 123 (1985).

(23) J.W. Stout, and L. H. Fisher, *J. Chem. Phys.* **9**, 163 (1940).

(24) F. Sohl, T, Spohn, D, Breuer and K. Nagel, *Icarus*, **157** 104-119 (2002).

(25) D. J. Stevenson, *Science*, **289** (5483): 1305-1307 (2000).

(26) Katrusiak, A., *Cryst. Res. Technol.* **26**, 523 (1991).

(27) G. Cooper , N. Kimmich , W. Belisle, et al. *Nature* **414** (6866): 879-883 (2001).

Table 1. Two-phase parameters of formic acid used to calculate the high-pressure melt curve

Parameter	Liquid-Phase	Solid-Phase
C_p (J/mole·K)	99.036	124.717
ΔH_0 (kJ/mole)	-425.100	-436.750
ΔS_0 (J/mole·K)	131.840	88.241
V_o (cc/g)	1.22	1.57
B_0 (GPa)	1.63	12.67
N	6.65	6.80